

pubs.acs.org/Biomac Article

# Design of Polymeric Thin Films to Direct Microbial Biofilm Growth, Virulence, and Metabolism

Trevor Franklin, Yinan Wu, Jiayan Lang, Sijin Li,\* and Rong Yang\*



Cite This: Biomacromolecules 2021, 22, 4933-4944



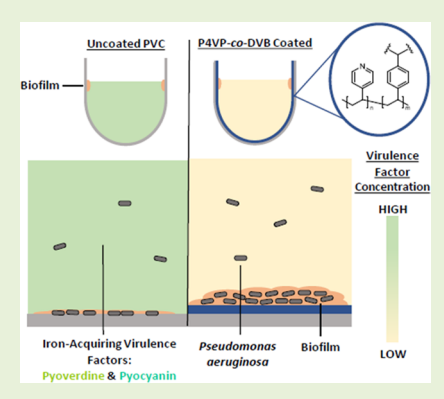
**ACCESS** 

Metrics & More

Article Recommendations

Supporting Information

ABSTRACT: Biofilms are ubiquitous in nature, yet strategies to direct biofilm behavior without genetic manipulation are limited. Due to the small selection of materials that have been used to successfully grow biofilms, the availability of functional materials that are able to support growth and program microbial functions remains a critical bottleneck in the design and deployment of functional yet safe microbes. Here, we report the design of insoluble pyridine-rich polymer surfaces synthesized using initiated chemical vapor deposition, which led to modulated biofilm growth and virulence in *Pseudomonas aeruginosa* (PAO1). A variety of extracellular virulence factors exhibited decreased production in response to the functional polymer, most significantly biomolecules also associated with iron acquisition, validating the material design strategy reported here. This report signifies a rich potential for materials-based strategies to direct the behavior of naturally occurring biofilms, which complement the existing genetic engineering toolkits in advancing microbiology, translational medicine, and biomanufacturing.



# ■ INTRODUCTION

Biological materials, including proteins, cells, and biomolecules, often coalesce and form functional communities at the interface with a surface, as exemplified by conditioning films, biofilms, and engineered tissue constructs. From the alternate vantage point, only under the extreme circumstance of a sterile environment can a human-engineered material avoid interaction with biological species. Accordingly, there is an inherent tie between surfaces and biological matter, and the directed engineering of materials involved in such biological interactions is at the heart of rich biomaterials research. A grand and critical challenge in biomaterials design is the ability to program cellular responses via precision material design. To control a diversity of programmable cellular behaviors, research on mammalian and stem cells has leveraged material properties such as surface energy, surface charge, stiffness, roughness, porosity, and biodegradability.

Programming the functions of bacteria via material design is an alluring yet uniquely challenging prospect. In nature, bacteria live predominantly in surface-associated communities known as biofilms that are found in nearly every ecosystem on Earth.<sup>7</sup> The vast abundance and rich biological functions of naturally occurring biofilms, if properly programmed, could be leveraged to treat microbiome disorders while minimizing complications, realize self-actuated water purification via coupled sensing and decomposition of contaminants, or enable novel soft robotics via programmed assembly.<sup>8–10</sup> Bacteria in biofilms are also valuable biosynthetic tools for small molecules or extracellular matrix components used by humans in edible, cosmetic, or medicinal products.<sup>11,12</sup> Genetically modified bacteria are the subject of promising applications in environ-

mental remediation and targeted biotherapeutic excretion, <sup>13,14</sup> yet they come with the risk of disturbing or devastating the ecosystem upon release to the natural environment. <sup>15</sup> By leveraging the robust environmental adaptability of microbes, programming microbial functions using precisely engineered functional materials emerges as a promising strategy to circumvent the environmental and health risks associated with genetically modified strains while tapping into the power of living organisms. For example, functional surfaces that reduce the pathogenicity of biofilms without killing the bacteria have the potential to enable the safe deployment of biofilms as self-repairing materials. <sup>16,17</sup>

Nevertheless, programming microbial phenotypes using functional materials (i.e., without genetic manipulation) presents unique challenges that are unprecedented in previous efforts, for example, on mammalian cells. Materials properties must be controlled with more precision due to the size of bacteria (volumes of nm³ to single-digit  $\mu$ m³), which makes in situ and real-time imaging a difficult yet circumventable challenge with the recent advances in microbial omics. 9 Most importantly, despite the ubiquity of biofilms in nature, laboratory culture of biofilms with reproducible phenotype/behavior has proven challenging. In contrast to the plethora

Received: June 7, 2021 Revised: October 4, 2021 Published: October 25, 2021





of antifouling polymers, materials enabling the stable growth of biofilms are scarce.<sup>21</sup> Extant research, therefore, has focused on materials that have been proven to support biofilm growth, such as poly(dimethylsiloxane), and variation of their physical properties. For example, surface stiffness has shown to influence adhesion strength, cell size, and antibiotic susceptibility of Pseudomonas aeruginosa and Escherichia coli. 22 Microstructures protruding from a flat surface were also shown to increase the propagation of flagellated cells when the structures were spaced at a density that maximized tangential microbe-structure collisions and minimized trapping of bacteria in circular trajectories.<sup>23</sup> While these examples serve as proof-of-principle for material-centric phenotype programming in microbes, they leave rich chemical properties, with a greater likelihood for sophisticated behavioral control, largely unexplored.

To enable control over functional phenotypes, we designed a pyridine-rich polymer (featuring precisely controlled crosslinking density to avoid dissolution) to support stable biofilm formation while suppressing pathogenicity. The design was based on the ability of pyridine rings to form strong yet dynamic ligand bonds with iron. Iron plays a critical role in many life-sustaining bio-redox reactions yet is scarcely present in the environment.<sup>24</sup> As an adaptive response to the scarcity of this vital element, microbes have evolved elaborate mechanisms to acquire iron, a common one of which hinges on the production and release of two classes of low-molecularweight compounds with high affinity to iron, namely siderophores and phenazines.<sup>25</sup> Due to the competitive iron uptake between microbial and mammalian cells (e.g., via transferrin), siderophores and phenazines are known to cause severe diseases such as neurotoxicity, amnesic poisoning, <sup>26</sup> and exacerbated infections. <sup>27</sup> The reported design of pyridine-rich surfaces enriched iron to the liquid-solid interface, supporting the growth of biofilms while reducing pathogenicity by suppressing the need to produce the disease-causing molecules. The simultaneous enhancement of biofilm growth and decrease in the production of iron acquiring molecules opposes the current understanding of a positive correlation between the two behaviors<sup>28</sup> and that between persistent biofilms and elevated pathogenicity. The research demonstrated a substantial advancement to the existing literature in biomaterials research, which has conventionally consolidated around efforts to kill or avoid the attachment of bacteria, whereas control over bacterial phenotypes via material design has rarely been attained.29

The basis of materials fabrication herein is initiated chemical vapor deposition (iCVD), an all-dry polymer thin film synthesis technique known for producing conformal coatings across substrate surfaces.<sup>30</sup> By using iCVD, a remarkably smooth and conformal coating could be achieved on curved bacteria culture microplates that would be difficult to achieve through a solution-based polymer synthesis technique,<sup>31</sup> where coatings tend to accumulate at the bottom of the well. Furthermore, the iCVD coatings support the reproducible and stable growth of biofilms due to the high purity of the functional polymeric coatings that arises from the one-step synthesis and application approach. The solvent-free nature of iCVD eliminates the need to remove impurities (e.g., solvents or catalysts) from the final product that would be exposed to bacteria during incubation. The iCVD approach is also substrate-independent, ensuring that surface conditions encountered by bacteria cultures in each well and on different

coated apparatuses were comparable and that information collected using disparate characterization methods was transferrable. Specifically, in addition to quantitative staining and infectivity assays to demonstrate enhanced biofilm formation and suppressed pathogenicity, the metabolic activities underlying those phenotypes were resolved using metabolomics, in which over 250 candidate biomolecules and/or fragments were analyzed.

This systematic study opens up a new topic in fundamental microbiology research of the biochemical behaviors elicited by functional materials, which is especially important given the ubiquity of synthetic materials in modern society. By systematically studying the behavioral and biochemical responses that arise from contact with precisely engineered materials, these new insights could direct the design of functional materials that enable the deployment of naturally occurring biofilms. Therefore, this work serves as proof-of-principle for the power of materials-based strategies to direct microbial functions, pointing to a new paradigm for engineering microbial functions and integration of microbes into the materials and devices used in everyday life.

#### **■ EXPERIMENTAL SECTION**

Polymer Thin Film Deposition via iCVD. All polymer coatings were deposited onto substrates of interest using a custom-built iCVD vacuum reactor (Kurt J. Lesker) featuring a cylindrical chamber with a radius of 25 cm and a height of 5 cm. Vapors of divinylbenzene (DVB) (Sigma-Aldrich, 80%) heated in a glass jar to 65 °C, 4vinylpyridine (4VP) (Sigma-Aldrich or Acros Organics, 95%) heated to 50 °C, and unheated tert-butyl peroxide (TBPO) (Sigma-Aldrich, 98%) were metered into the reactor chamber at flow rates established by a heated mass flow controller (MFC) (1152C, MKS Instruments), a needle valve, and an unheated MFC (GE50A, MKS Instruments), respectively. All chemical reagents were used as received without alteration. Another manifold regulated by an unheated MFC was used to supply argon to promote flow and mixing of all vapor reagents. Vacuum conditions in the reactor chamber were facilitated by a twostage rotary vane vacuum pump (E2M40, Edwards), and a pressure setpoint measured by a capacitance manometer (627B, MKS Instruments) was controlled by a throttle valve (235B, MKS Instruments). Silicon (Si) wafers (Pure Wafer) and 96-well microplates (2797/3370/3916, Corning) onto which films were deposited were placed atop a stage in the reactor chamber that was held at a chosen temperature controlled by a recirculating chiller (Accel 500 LT). The partial pressure of each monomer in the reactor chamber was controlled to be at a fraction of its saturation pressure in order to avoid condensation at the substrate surface that would yield nonuniform coverage (e.g., pinholes on the microplates). Roundbottom microplates were rested on a custom aluminum holder that extended the chilling capacity across the entirety of the topographically complex substrate. A filament array (55% Cu/45% Ni, Goodfellow) heated by a DC power source (1715A, B&K Precision) and positioned 2 cm above the substrates split the TBPO into tertbutoxide radicals that initiated polymerization upon contact with monomers adsorbed to the cooled substrates below. Type K thermocouples (Omega Engineering) monitored the substrate stage and filament array temperatures, while an in situ 633 nm heliumneon laser interferometer (JDS Uniphase) provided real-time measurement of the polymer film thickness.

**Polymer Thin Film Characterization.** Polymer coating thickness resulting from each deposition was measured on the Si wafers using a J.A. Woollam alpha-SE ellipsometer. Measurements were collected in standard mode at incident angles of 65, 70, and 75° with 180 wavelengths used across a range of 380–900 nm, and a Cauchy–Urbach model was used to fit the data.

FTIR spectroscopy was performed using a Bruker VERTEX Series V80v spectrometer in transmission mode. Spectra were recorded

using a mercury cadmium telluride detector across the range of 600—3400 cm<sup>-1</sup> with a 4 cm<sup>-1</sup> resolution and were background corrected using an uncoated Si wafer. The plotted spectra were averaged over 128 scans and baseline corrected.

**Cell Culture Conditions.** Cells of *P. aeruginosa* (PAO1) (ATCC 47085) were transferred from a -80 °C freezer stock onto a tryptase soy agar plate and incubated overnight at 37 °C. Using an inoculation loop, a single colony was removed from the plate and placed into 5 mL of lysogeny broth (LB) medium, which was incubated at 37 °C and shaken overnight for 16 h. To prepare iron-excess medium, 77  $\mu$ L of 1.85 mM sterile iron(III) chloride stock solution was added to 7 mL of LB medium to obtain a final iron concentration of 20  $\mu$ M. To prepare iron-deprived medium, 2.5 mg of 2,2′-bipyridyl (≥99%, Sigma-Aldrich) was added to 5 mL of LB medium and filtered through a 0.2  $\mu$ m filter into 35 mL of additional LB to make a 400  $\mu$ M stock solution. 70  $\mu$ L of the overnight PAO1 culture was diluted (1:100) into 7 mL of fresh LB medium, iron-excess medium, and iron-deprived medium to prepare test cultures under the 3 conditions.

Biofilm Growth Assay. Prior to inoculation for a 24 h culture, poly(4-vinylpyridine-co-divinylbenzene) (P4VP-co-DVB) coated, PDVB coated, and uncoated round-bottom 96-well microplates and lids were sterilized by UV exposure for 1 h. After mixing well, 150  $\mu$ L of diluted overnight culture medium from each condition (unaltered LB, iron-excess, and iron-deprived) was added to wells of the uncoated and coated microplates. Fresh LB medium with no PAO1 culture was also added to each microplate as a control. Each microplate was covered with a lid to limit evaporation and incubated at 37 °C for 24 h. By removing the cell culture medium (150  $\mu$ L) from the microplates after 24 h, biofilms were left on the walls of the wells, and these plates were used for biofilm growth quantification. The well plate was submerged and shaken in a bin of purified water to remove all nonadhered cells and leave only biofilms behind. Rinsing was repeated three times with fresh water. Next, 200 µL of crystal violet solution (0.5% w/w in water) was added to each well to stain the biofilms for 15 min. Following removal of the dye with a pipette, the excess dye was rinsed off of the biofilms by submerging and shaking the well plate in a bin of purified water. The dye-rinsing step was repeated with fresh water, and the microplates were left to dry for at least 3 h. Once dry, 200 µL of 30% acetic acid was added to each well to dissolve the stained biofilms for 15 min. The solution containing the dissolved dye was transferred to a flat-bottom microplate, and absorbance at 550 nm was recorded on a Tecan Infinite M1000 Pro plate reader.

Virulence of PAO1 Culture Supernatants toward Human Fibroblasts. Human primary dermal fibroblasts (ATCC PCS-201-012) were maintained in Fibroblast Basal Medium (FBM, ATCC PCS-201-020) with Fibroblast Growth Kit-Low Serum (ATCC, PCS-201-041) and 1% penicillin/streptomycin (Gibco). The fact that P. aeruginosa is a pathogen in skin infections directed the choice of primary dermal fibroblasts, a common cell line for PAO1 virulence assays. 32,33 The cells were subcultured into the wells of a 96-well microplate (Corning, 3596) and grown to 100% confluence over the course of 24 h. The medium was removed from the fibroblast culture wells, and the cells were rinsed with phosphate-buffered saline. Test wells were filled with 100  $\mu$ L of the aforementioned medium, but lacking antibiotics, and 50  $\mu$ L of supernatant from the coated and uncoated culture wells that was collected during the Metabolomics Analysis. Controls consisted of either fibroblast medium supplemented with 10% Triton X or 150  $\mu$ L of FBM with no cells. Following 24 h of incubation at 37 °C and 5% CO2, the lactate dehydrogenase (LDH) cytotoxicity assay kit (Cayman Chemical, 601170) procedure was followed for a colorimetric analysis. Absorbance at 490 nm was recorded using the plate reader.

**Metabolomics Analysis.** Sterilization and inoculation of microplates with 16 wells for each medium condition followed the procedure of the Biofilm Growth Assay. After 24 h of incubation, the culture medium was removed from each well and stored in microcentrifuge tubes for absorbance/fluorescence analysis, leaving behind only biofilms in the microplate wells. 200  $\mu$ L of 10% acetic acid in methanol was added to each of the sample-containing wells to

dissolve the biofilms for 30 min, during which the plates were covered and placed in a freezer at −20 °C to prevent evaporation. Solutions from four adjacent wells at each culture condition were combined into one microcentrifuge tube for a combined 800  $\mu$ L of solution with dissolved biofilm. Repeating this to use all 16 samples from each culture condition produced 4 microcentrifuge samples from each culture condition (unaltered LB, iron-excess, and iron-deprived) on the uncoated plate and the coated plate. The capped microcentrifuge tubes were immersed in ice and sonicated for 20 min prior to centrifuging at 14,000g for 20 min. The supernatant was collected from each centrifuge tube and placed into fresh microcentrifuge tubes for another round of centrifugation at 17,000g for 20 min. The supernatants were again transferred to fresh microcentrifuge tubes and stored in a freezer at -20 °C until liquid chromatography coupled to quadrupole time of flight (LC/Q-ToF) mass spectrometry analysis was performed.

The metabolomics samples were analyzed by reversed-phase chromatography on an Agilent 1260 HPLC, using a ZORBAX RRHD Eclipse Plus C18 column (Agilent) with 2  $\mu$ L injection of each sample. The mobile phase was water (A) and acetonitrile (B), both with 0.1% (v/v) formic acid. The elution procedure was 1% B between 0 and 5 min, 1–99% B between 5 and 45 min, 99% B between 45 and 50 min, 99–1% B between 50 and 53 min, and 1% B between 53 and 60 min with a flow rate of 0.5 mL/min. A coupled Agilent 6545 Accurate-Mass Q-TOF ESI mass spectrometer was used to collect MS data in positive mode. After that, the resulting raw metabolomic data were subjected to the XCMS cloud-based online platform (https://xcmsonline.scripps.edu/) to conduct a paired two-group test.

**Identification of Targeted Metabolomics Compounds.** This experiment was also performed by LC/Q-ToF spectrometry (Agilent) using the ZORBAX RRHD Eclipse Plus C18 column (Agilent) in MS mode with 1  $\mu$ L injection of experimental samples and standards for pyochelin, phenazine-1-carboxylic acid (PCA), and rhamnolipids. The mobile phase was water (A) and acetonitrile (B), both with 0.1% (v/v) formic acid. The elution procedure was 5% B between 0 and 1 min, 5–95% B between 1 and 11 min, 95% B between 11 and 13 min, 95–5% B between 13 and 14 min, and 95% B between 14 and 16 min with a flow rate of 0.4 mL/min.

The standards were dissolved in methanol to make stock solutions at a concentration of 1 g/L for pyochelin, 0.1 g/L for phenazine-1-carboxylic acid, and 10 g/L for rhamnolipids. The stock solutions were diluted to appropriate concentrations for sample preparation.

Pyoverdine and Pyocyanin Assays. Sterilization and inoculation of microplates with 16 wells at each medium condition followed the procedure of the Biofilm Growth Assay. Each microplate was covered with a lid to limit evaporation and incubated at 37 °C for 24 h. Following incubation, the medium was removed from four adjacent wells and combined into a 1.5 mL microcentrifuge tube, creating 4 microcentrifuge tube samples for each medium condition. The contents of each tube were mixed, and 200 µL was transferred to a flat-bottom 96-well microculture plate for an  $\mathrm{OD}_{600}$  measurement on a Tecan Infinite M1000 PRO plate reader and then transferred back to the tube. The tubes were centrifuged for 15 min at 10,000g. 200  $\mu$ L of the supernatant was added to a black flat-bottom 96-well microplate used to record fluorescence data on the plate reader, and the same volume was added to a clear flat-bottom 96-well microplate to record absorbance data. Pyoverdine fluorescence was measured with an excitation wavelength of 405 nm and an emission wavelength of 460 nm. Pyocyanin absorbance was recorded at 695 nm.

Time-Lapse Pyoverdine Assay. A P4VP-co-DVB coated black 96-well microculture plate and lid were sterilized by UV exposure for 1 h. After mixing well, 150  $\mu$ L of the diluted culture in unaltered medium was added to 16 wells, and LB medium with no PAO1 was added to 8 wells as a control. The lid was added, and the sides were wrapped tightly in Parafilm to deter evaporation. After a 37 °C environment was established and stabilized in the plate reader, the plate was inserted and fluorescence (excitation—405 nm and

emission—460 nm) was recorded every 15 min for 14 h. The same procedure was repeated for an uncoated black 96-well microplate.

**Time-Lapse Biofilm Assay.** Prior to inoculation, P4VP-co-DVB coated and uncoated round-bottom 96-well microculture plates and lids were sterilized by UV exposure for 1 h. After mixing well, 100  $\mu$ L of the diluted overnight culture in LB medium was added to 6 wells on 6 rows (total of 36 wells) on the uncoated microplate and on the coated microplate. Each microplate was covered with a lid to limit evaporation and incubated at 37 °C. Every hour for 6 h, one 6-well strip was cut from each incubating microplate and subjected to the aforementioned Biofilm Growth Assay altered only by using 230  $\mu$ L of crystal violet solution and acetic acid solution.

Biofilm Imaging. Prior to inoculation, P4VP-co-DVB coated and uncoated round-bottom 96-well microculture plates and lids were sterilized by UV exposure for 1 h. After mixing well, 150  $\mu$ L of diluted overnight culture medium from unaltered and iron-excess conditions was added to 16 wells on the uncoated and coated microplates. Each microplate was covered with a lid to limit evaporation and incubated at 37 °C for 24 h. Following incubation, cell culture medium was removed from the wells to leave behind biofilms that were fixed for SEM analysis. The wells were filled with 2% glutaraldehyde in 0.05~Msodium cacodylate buffer for 2 h, followed by three rinses with buffer. The contents of the wells were then dehydrated using 10 min exposures to ethanol concentrations of 25, 50, 75, and 100%. The wells were filled with 100% ethanol to dry overnight, and drying was completed using critical point drying. Segments of wells from each medium condition were cut, fixed to a stage with copper tape, and sputtered with a few nanometers of gold/palladium. SEM analysis was performed on a Zeiss Gemini SEM 500 with an acceleration voltage of

**Polymer Coating Stability.** Five wells of a P4VP-co-DVB coated well plate were filled with deuterium oxide (99.9%, Cambridge Isotopes Laboratories) and covered with a lid to deter evaporation before placing in an oven set to 37 °C overnight to mimic culture incubation conditions. The solvent was then transferred to a clean NMR tube for <sup>1</sup>H analysis using a Bruker AV-500.

ICP-MS Analysis of Surface Enriched Iron. The wells of one full P4VP-co-DVB coated and one uncoated microculture plate were filled with 200  $\mu$ L of LB medium and allowed to soak for 3 h. Following the soaking, LB medium was removed and each microplate was washed five times with purified water. The soaked microplates and an unsoaked control were delivered to the Trace Elements Clean Lab at the University of Wisconsin-Madison Wisconsin State Laboratory of Hygiene for detailed analyses on surface iron content under each condition. Each well of the microplates was extracted by adding 200  $\mu$ L of 1 M HCl (Optima) and shaking for 19 h. The liquid from 24 wells was combined to form one sample such that each microplate yielded 4 replicates of each condition. Quantitative analysis of iron-56 was performed using a magnetic-sector inductively coupled plasma mass spectrometer (Thermo-Finnigan Element XR) with four replicates for each condition. A mean batch specific analytical blank with outlier detection was applied to all sample data.

**Statistical Analysis.** Mann—Whitney  $\hat{U}$  tests (two-tailed) were used to determine whether the values yielding the absorbance/fluorescence averages on coated and uncoated substrates were statistically significant. In the metabolomics analysis, statistical significance was calculated using paired, two-group Welch's t-tests.

# ■ RESULTS AND DISCUSSION

**Deposition of Insoluble P4VP-co-DVB Surfaces onto Bacteria Culture Substrates Using iCVD.** Due to the vitalness of iron, *P. aeruginosa* has developed a variety of mechanisms for acquiring it, including production and deployment of siderophores, the ferrous iron transport (Feo) system that relies on phenazines for iron reduction and transport, and direct uptake of dissolved heme molecules.<sup>35</sup> In order to modulate these iron acquisition activities, our design positioned iron-enriching pyridine functional groups where

cells that form biofilms are settling while scavenging for iron, thus creating a surface favorable for growth yet discouraging for the production of the iron-scavenging pathogenic molecules

The iron-enriching functional materials studied herein were synthesized using the iCVD technique in which vapor phase reagents yielded polymer thin films through free radical polymerization. In this work, 4VP was copolymerized with a DVB cross-linker to prepare P4VP-co-DVB thin films. The pyridine presented by the repeating unit of 4VP in the copolymer coating was designed to coordinate with iron and thereby reduce iron scavenging activities of surface-attached *P. aeruginosa* (PAO1 strain). The DVB cross-linker was included as a comonomer to render the resultant coating insoluble when submerged in culture medium or other solutions required in characterizations, the stability of which was confirmed by NMR (Figure S1).

To coat a substrate with P4VP-co-DVB, substrates were placed into a custom-built iCVD reactor chamber maintained at 400 mTorr on a temperature-regulated stage that was maintained at 25 °C (Figure S2). Monomers of 4VP and the DVB cross-linker were metered into the chamber at a ratio of approximately 12:1. A TBPO initiator was delivered into the reactor simultaneously with the monomers and thermally decomposed into two free radical species (tert-butoxide) by a heated filament array suspended over the temperaturecontrolled stage. Impingement of the radicals with monomers adsorbed to the substrate initiated polymerization, which gave rise to the growth of P4VP-co-DVB thin films. The thickness of the thin films was determined in real time by in-situ interferometry performed on a Si wafer, which was placed in the reactor chamber adjacent to the substrates to be coated (e.g., microplates).

Three types of substrates were coated using the iCVD technique: Si wafers for the aforementioned in situ coating thickness control and materials characterization, round-bottom microplates [made of polyvinyl chloride (PVC)] for quantification of biofilm growth, and flat-bottom microplates (made of polystyrene) for monitoring the real-time release of microbial iron scavengers (e.g., pyoverdine). The round-bottom microplates were subjected to the iCVD treatment until a 600 nm P4VP-co-DVB film was achieved on an adjacent Si wafer, which ensured that all surfaces of the microplate were coated (Figure S3). The flat-bottom microplates were coated until a thickness of 1600 nm was achieved on an adjacent Si wafer. The iCVD technique is known for its substrate independence, which ensures identical physicochemical properties of the P4VP-co-DVB coatings on all treated substrates <sup>36</sup>

FTIR spectroscopy was used in transmission mode to analyze the composition of the iCVD P4VP-co-DVB coatings (on Si wafers). Peaks associated with both 4VP and DVB were observed, including those indicative of vibrations of the pyridine ring of 4VP at 1597, 1557, 1493, 1453, and 1415 cm<sup>-1</sup>.<sup>37</sup> The percentage of the DVB cross-linker in each coating was determined using the area of the peak at 710 cm<sup>-1</sup> belonging to the C–C vibration of the phenyl moiety of DVB. The peak at 710 cm<sup>-1</sup> was normalized by the thickness of the copolymer and subsequently divided by the thickness-normalized peak area of the PDVB homopolymer (Figure S4) to yield the percentage of DVB in the copolymer. Insoluble, cross-linked P4VP-co-DVB coatings in the experiments described herein contain approximately 80% 4VP and

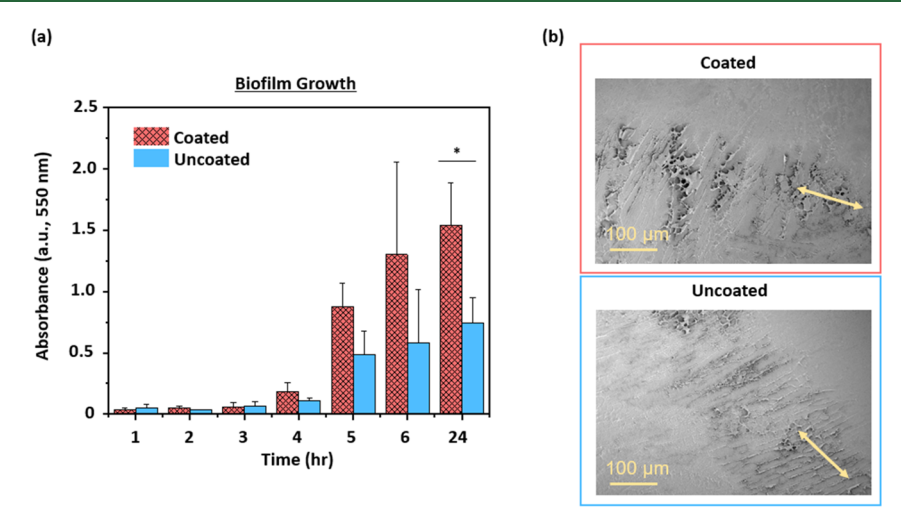


**Figure 1.** PAO1 biofilm growth on coated and uncoated substrates. (a) Biofilm growth at hourly increments over the course of 6 h (n = 12) and at 24 h (n = 32) of incubation on coated and uncoated microplates ( $p = 2.3 \times 10^{-15}$ , \*). (b) SEM images of PAO1 biofilms on P4VP-co-DVB coated and uncoated substrates incubated in LB medium. The double-sided arrow represents the air—liquid interface.

20% DVB cross-linker, and experimental samples covered in this thin film are referred to as "coated" going forward. An FTIR spectrum and deposition conditions for the PDVB homopolymer used in control experiments are shown in Figure S5.

Enhanced Formation of PAO1 Biofilms on the P4VP-co-DVB Coating. Enhanced biofilm formation on coated surfaces was demonstrated by incubating PAO1 cultures at 37 °C in P4VP-co-DVB coated and uncoated 96-well round-bottom microplates. In the following, unless specified otherwise, cultures were incubated for 24 h post-inoculation because PAO1 is commonly known to form biofilms at the solid—liquid—air interface within 8 h, and in our experience, the culture duration of 24 h gave rise to stable and reproducible PAO1 biofilms with minimal dispersion (reported to occur after several days). 38,39

Biofilm growth of PAO1 on coated/uncoated microplates was quantified using a crystal violet-based protocol.<sup>40</sup> In brief, biofilms were rinsed to remove planktonic cells and stained with crystal violet prior to dissolving the stained biofilms in acetic acid solution for spectroscopic analysis. Absorbance at 550 nm (i.e., the wavelength of the crystal violet stain) was proportional to the amount of PAO1 biofilms because loosely attached bacteria had been removed by rinsing and the treatment with acetic acid released the crystal violet taken up by the biofilms. At the end of the 24 h incubation, the amount of PAO1 biofilms adhered to the coated substrates was over 2 times that measured on uncoated substrates, with OD<sub>550</sub> values of 1.54  $\pm$  0.35 a.u. (coated) and 0.75  $\pm$  0.21 a.u. (uncoated) (Figure 1a). Biofilm growth was further evaluated on an hourly basis over the first 6 h of incubation on coated and uncoated microplates to reveal that the twofold difference in growth rate on the coated/uncoated substrates started to emerge as early as the fourth hour (Figure 1a), which persisted for all subsequent time points and up to 24 h.

The biofilms obtained after 24 h of incubation on coated and uncoated substrates were subsequently fixed for visual analysis via SEM. Visible in the images (Figure 1b) was the difference in architecture, which resulted from the enhanced growth of biofilms on the coated surfaces. Specifically, biofilms on the coated surfaces developed more substantial three-dimensional architecture, that is, with vertical growth giving

rise to features that extended farther away from the surface compared to uncoated surfaces. This increase agrees with the established positive correlation between iron levels and biofilm growth, which validates our materials design approach. Given the results of these experiments, P4VP-co-DVB can be used to culture PAO1 for heightened biofilm growth and to potentially direct biofilm growth according to a predetermined pattern of the coating.

Reduced Pathogenicity to Human Dermal Fibroblasts due to P4VP-co-DVB Exposure. Reduced pathogenicity of PAO1 biofilms grown on coated surfaces was demonstrated by collecting supernatants of cultures grown on coated and uncoated microplates to treat human primary tissue cells using established virulence assays. 42 Supernatants collected from PAO1 cultures in coated and uncoated microplates were added to fibroblasts that had been cultured in FBM to 100% confluency (over 24 h). After an additional 24 h of incubation with PAO1 culture supernatants, cell death was assessed using a LDH cytotoxicity assay. The absorbance at 490 nm, corresponding to formazan, was converted to a percentage of cell death by normalizing that absorbance using a control group that represented 100% cell death, achieved by supplementing the FBM with 10% Triton X (Figure 2). Exposure to supernatants of cultures from coated microplates led to measured lethality that was 6.78% of the control compared to 20.93% for those obtained from the uncoated microplates. The P4VP-co-DVB coating reduced PAO1 pathogenicity to 32.39% of the PAO1 cultures grown on uncoated culture plates.

These results indicate a reduced risk of skin infection, among numerous health complications PAO1 biofilms can cause, when grown on the P4VP-co-DVB surfaces. The simultaneous increase in biofilm growth and decrease in pathogenicity are distinct from previously reported effects of soluble species on PAO1 biofilms, 43 where interventions that decreased virulence invariably led to the reduced amount of biofilm. We attributed the unusual decrease in virulence to the decreased accumulation of the molecules associated with iron acquisition, as indicated by the fluorescence/absorbance spectroscopy and metabolomics analysis detailed below.

Decrease in Release of Siderophore and Phenazine Due to P4VP-co-DVB Exposure. The P4VP-co-DVB func-

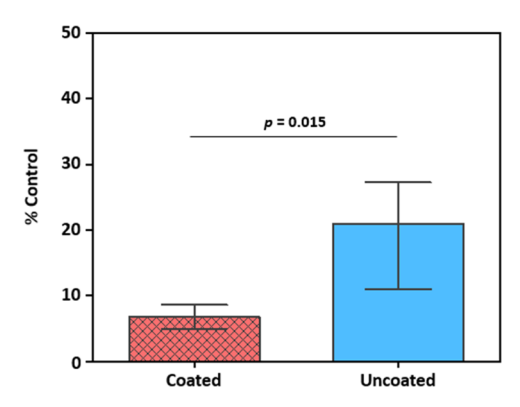


**Figure 2.** Cytotoxicity of human fibroblast cells exposed to PAO1 culture supernatants. The cytotoxicity of PAO1 culture supernatants from cultures grown in coated and uncoated microplates was assessed for 24 h on human dermal fibroblast cells. The results are expressed as the percentage of absorbance at 490 nm compared to a control sample in which all cells were killed (n = 8).

tional coating was designed to decrease the production of iron scavenging molecules by providing an iron-rich surface for the settling/growing of PAO1 biofilms. That ability was directly supported by the observation of a distinct color difference between cultures in coated wells that lacked the blue-green hue compared to cultures in uncoated wells (Figure S6). This blue-green color is a signature of *P. aeruginosa* cultures and has been attributed to the production of (i) yellow-green pyoverdine, a siderophore secreted to scavenge for iron in the local environment, <sup>35</sup> and (ii) blue-green pyocyanin, a virulence factor and phenazine produced to complement the side-rophore-based iron uptake mechanism.<sup>35</sup>

Pyoverdine, the primary siderophore of PAO1 and one of the strongest known iron-binding biomolecules, has previously been a target for regulation by soluble species because of its multifaceted role in influencing the growth and metabolism of *P. aeruginosa*.<sup>25,44</sup> Once a siderophore has sequestered iron extracellularly, it may be taken up by *P. aeruginosa* for use in life-sustaining oxidation—reduction metabolic reactions.<sup>45</sup> The binding affinity of siderophores to iron is superior to mammalian Fe<sup>3+</sup>-binding molecules such as transferrin, thus allowing the bacteria to steal iron from a mammalian host,

which in turn contributes to their pathogenicity.<sup>46</sup> Though the primary purpose of pyoverdine is to compete for iron that can be used by *P. aeruginosa*, pyoverdine also functions to protect the microbe from heavy metals via sequestration or from UV damage by absorbing radiation and hence reducing reactive oxygen species. Pyocyanin is a virulence factor with multiple antimicrobial and antifungal capabilities, including inhibition of cellular respiration, in addition to its association with iron uptake through the Feo system.<sup>35,47–49</sup> The released levels of pyoverdine and pyocyanin into the cultures from coated or uncoated microplates were further characterized as described below.

Following 24 h of incubation, culture medium from each well was centrifuged in order to isolate the supernatant for spectroscopic analysis. Pyoverdine was quantified via fluorescence spectroscopy with an excitation wavelength of 405 nm and an emission wavelength of 460 nm. The amount of pyoverdine released into the culture in coated microplates was reduced to 64.31% of the amount released in uncoated microplates, with the fluorescence intensity of 12,197.25  $\pm$ 4152.02 a.u. (coated) and 18,966.42 ± 5378.78 a.u. (uncoated) (Figure 3a). Pyocyanin was quantified by using absorbance spectroscopy at a wavelength of 695 nm (Figure 3b). Similar to the case of pyoverdine, pyocyanin absorbance was decreased in supernatants of the cultures incubated in coated microplates to 78.18% of the absorbance measured in supernatants from uncoated microplates, with the OD<sub>695</sub> values of 0.12  $\pm$  0.015 and 0.15  $\pm$  0.0093 a.u., respectively.

To assess the time-evolution of the effect of the coating on the release of microbial iron scavengers, the release level of pyoverdine was monitored in real time for 14 h, a window of time sufficient to capture the distinct release profiles on the coated versus uncoated surfaces (Figure 3c). During the first 2 h of incubation, levels of pyoverdine remained at a basal level, that is, approximately 30 a.u., on both surfaces, which subsequently decreased during the 3rd and 4th hours to below the detection limit. This decreased pyoverdine level coincided with the initiation of detectable biofilm growth (Figure 1a) and could thus be attributed to the increased consumption of the initial stock of iron-bound pyoverdine (which was introduced along with the overnight culture during inoculation, see Experimental Section for details). The release

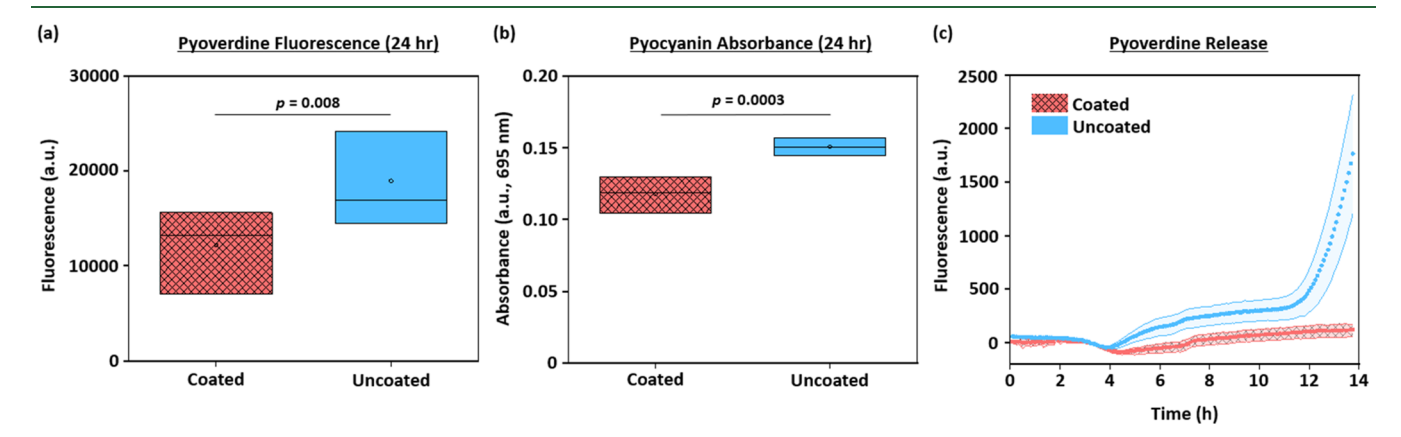


**Figure 3.** Spectroscopic assays quantifying PAO1 pyoverdine and pyocyanin production in standard LB medium. (a) Fluorescence of pyoverdine released into culture medium by PAO1 within coated and uncoated microplates in standard LB broth (n = 12). (b) Absorbance of pyocyanin released into culture medium by PAO1 within coated and uncoated microplates in standard LB broth (n = 8). Data in (a-b) are represented by an interquartile range (box), median (line), and mean (dot). (c) Time-lapse quantification of pyoverdine released into cultures in LB medium within coated and uncoated microplates (n = 16, dot = mean, and band = SD).

profiles on the coated and uncoated surfaces diverged after the 4th hour. For the uncoated surface, the pyoverdine release level steadily increased to  $323.75 \pm 106.03$  a.u. by the end of the 11th hour, which was followed by a drastic increase with the fluorescence intensity nearly doubling each hour, reaching  $1765.65 \pm 553.68$  a.u. by the end of the 14th hour. For the coated surface, the pyoverdine release level remained low (at below the detection limit) by the end of the 7th hour and subsequently started to increase slowly to reach a fluorescence intensity of  $115.50 \pm 57.51$  a.u., 6.54% of the uncoated level by the end of the 14 h incubation.

The decrease in the production of siderophores and phenazines atop coated plates indicated a reduced need to scavenge for iron, hinting at a bio-cooperative rather than a competitive role of P4VP-co-DVB with PAO1 biofilms, which could be explained by their relative affinities for dissolved iron. Pyridines have a moderate binding affinity for iron (e.g., the binding energy for a pyridine-Fe complex is  $\sim$ 621 kJ/mol), <sup>50</sup> thus capable of enriching iron from surroundings onto the surface. The enrichment of nutrients like iron and other macromolecules that form a conditioning film happens almost immediately after submersion into the aqueous solution.<sup>51</sup> Although the formation of a conditioning film (i.e., a layer of proteins, nutrients, and other macromolecules that gravitate toward a submerged surface) may seem to compromise the effectiveness of the surface-enriched iron, a conditioning film should, in fact, be viewed as integral to the outcome captured in this report. This is because the specific chemical and structural properties of a surface create preferential affinities for different molecules dissolved in the surroundings, hence creating a conditioning film unique to that surface.<sup>5</sup>

To observe this effect in LB medium, ICP—MS was used to quantify iron on the coated and uncoated microplates after soaking in LB medium for 3 h (Figure S7). Iron was 6.1 times as abundant on average on the coated microplate than the uncoated microplate after soaking in LB medium, indicating that this dynamic is due to the polymer coating. This high surface iron content was indeed a result of the enrichment of iron by P4VP-co-DVB as the medium exposure led to a 2.1-fold increase on average in the surface iron content on the coated microplate.

The surface-bound Fe, positioned conveniently for uptake via the Feo system in surface-attached PAO1, could thus meet the need for intracellular iron and decrease siderophore- and phenazine-based scavenging by the biofilms. Alternatively, surface-bound Fe may be "stolen" by pyoverdine due to its high affinity for Fe (>5000 kJ/mol). 54 Furthermore, concentrating iron to the surface could improve the efficiency of the pyoverdine-based system in PAO1 biofilms because it enables siderophores to travel less distance to shuttle iron. The combined effect of enhanced biofilm growth and siderophore release suppression is unique because biofilm growth and pyoverdine production are known to have a positive correlation, where iron acquisition supports biofilm growth that in turn spurs pyoverdine synthesis. 28,55 Pyoverdine and pyocyanin production and biofilm growth were also assessed on microplates coated with a homopolymer of PDVB. Without the pyridine side groups, the release of pyoverdine and pyocyanin from cultures was not suppressed and biofilm growth was not enhanced compared to the uncoated microplates (Figure S8). Accordingly, the unique behavior of enhanced biofilm growth with decreased release of iron

scavenging biomolecules can be attributed to the 4VP moiety and its iron-coordinating ability.

Alteration of the Biofilm Environment from Interaction with P4VP-co-DVB Revealed by Metabolomics. Metabolomics was utilized to systematically study the small molecule metabolism of biofilms grown on coated versus uncoated substrates. To isolate the response of biofilms, liquid culture containing planktonic cells was removed after 24 h of incubation to leave behind the surface-attached biofilms for metabolomics analysis. Biofilms were subsequently dissolved and processed such that cells contained within would be lysed prior to extraction of small molecules for analysis by LC/Q-ToF spectrometry to detect changes in small biomolecules present in biofilms grown on P4VP-co-DVB coated or uncoated microplates. A total of 272 candidate biomolecules and/or fragments were identified through a paired two-group test that focused on molecules that differed significantly (foldchange > 2, p < 0.01) in production in the biofilm due to the coating. To ensure the accuracy of the molecules identified that were both abundant and significantly different, commercially available pure products were used as standards (Figure S9). The three metabolites highlighted below were selected for their abundance in addition to the significant fold change in response to the coating, and a full list of the identified candidate biomolecules and/or fragments is given in Table S1.

Metabolomics captured reduced levels of two components that are critical to the iron acquisition behavior of PAO1 on the coated surfaces: pyochelin and PCA. Similar to pyoverdine, pyochelin is a siderophore (i.e., an iron scavenger excreted by *P. aeruginosa*). The level of pyochelin within biofilms grown on coated substrates was 34.60% of the level on uncoated substrates (Figure 4), which was calculated for the total biofilm content present in the coated or uncoated wells.

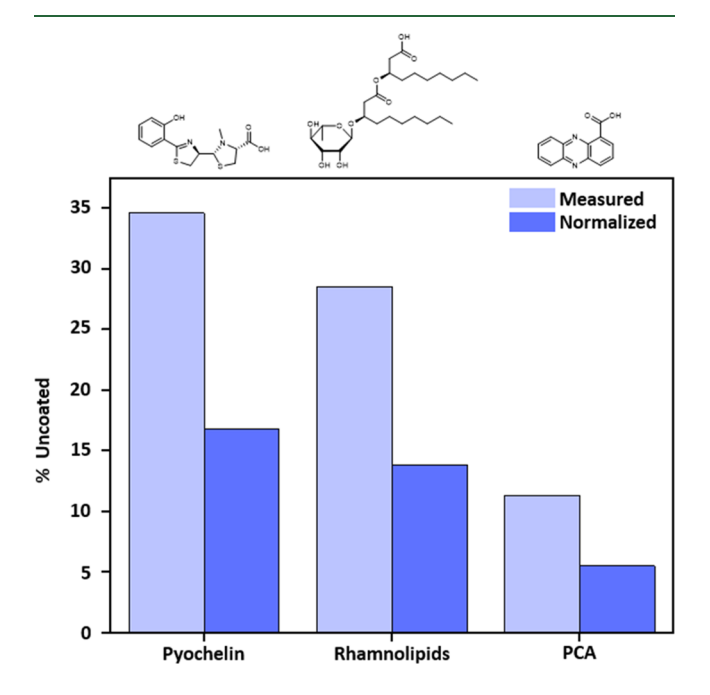


**Figure 4.** Metabolomics characterization of targeted molecules in PAO1 biofilms. LC/Q-ToF led to the identification of three target compounds with structures represented here. The amount of the molecule found in biofilms grown on coated substrates is displayed as a percentage of the amount on uncoated substrates, along with the percentage normalized by average biofilm growth (n = 4).

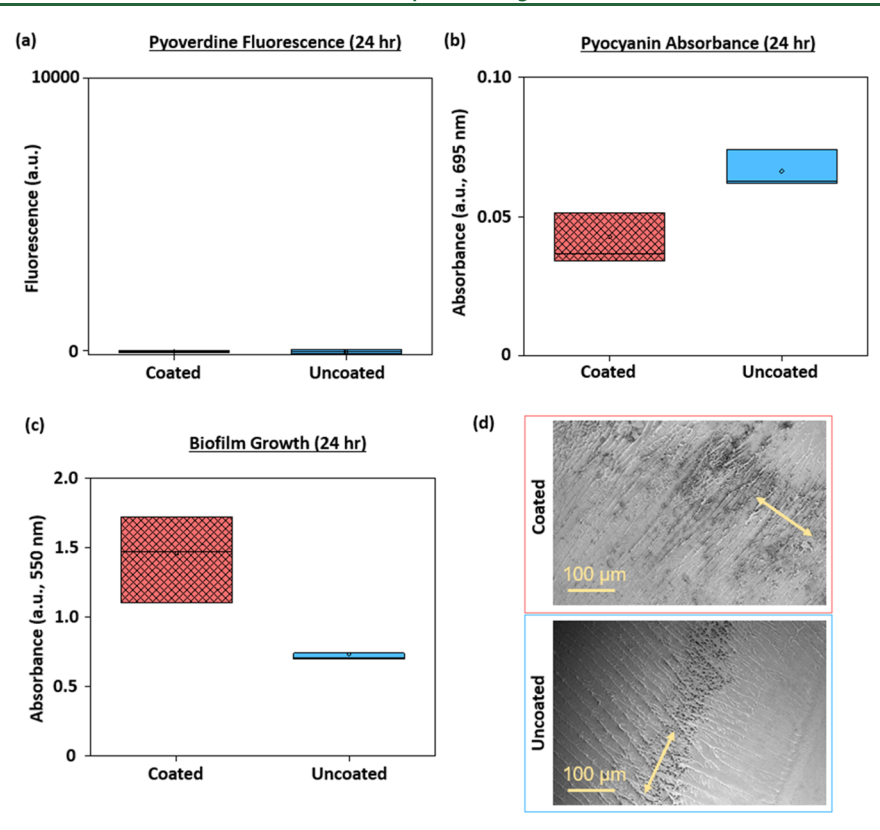


Figure 5. Spectroscopic assays quantifying PAO1 pyoverdine and pyocyanin production in iron-excess medium. (a) Fluorescence of pyoverdine released into culture medium by PAO1 within coated and uncoated microplates in iron-excess broth (n = 8). (b) Absorbance of pyocyanin released into culture medium by PAO1 within coated and uncoated microplates in iron-excess broth (n = 4 for coated and n = 3 for uncoated). (c) PAO1 biofilm growth on coated and uncoated microplates in iron-excess broth (n = 16). Data in (a-c) are represented by an interquartile range (box), median (line), and mean (dot). (d) SEM images of PAO1 biofilms on P4VP-co-DVB coated and uncoated substrates incubated in iron-excess medium. The double-sided arrow represents the air-liquid interface.

Because biofilms on the coated substrates grew to be 206% larger in comparison to those on uncoated substrates according to the crystal violet assay, the level of pyochelin in coated wells was 16.81% of the level in uncoated wells when normalized by the biofilm quantities under each condition. PCA is a precursor in the synthetic pathway to produce pyocyanin, another phenazine and toxin, and is also capable of redox-cycling extracellular iron for uptake via the Feo system. The total level of PCA produced in biofilms grown on coated substrates was 11.33% of the level on uncoated substrates, which became 5.50% when normalized by the difference in the biofilm quantity.

The coating also led to significantly lowered rhamnolipid content in biofilms. Rhamnolipids are an important class of glycolipids produced by P. aeruginosa that have been speculated to perform a broad range of bacterial functions, such as increasing virulence, increasing swarming motility, and enabling dispersal.<sup>57-59</sup> Among the rhamnolipids, the metabolomics performed here identified mono-rhamnolipids with a single rhamnose group and  $C_{10}-C_{10}$ ,  $C_8-C_{12}$ , or  $C_{12}-C_8$  side chains to have the most significant change in accumulation in response to the coating. Their average accumulation level in biofilms grown on coated microplates was 28.49% of the level on uncoated ones, corresponding to 13.83% when normalized by the amounts of biofilm grown on each surface. These results are consistent with previous findings that rhamnolipid synthesis is increased when iron is limited, and increased rhamnolipid production has shown to result in flatter biofilms

that lack microcolony formation due to increased twitching motility.  $^{58}$ 

The three molecules highlighted above were selected for the combination of the statistically significant fold change, high abundance (mass), and relationship to the iron acquisition behavior. Decreased accumulation of pyochelin and PCA corroborated the dampened iron scavenging behavior. In total, 272 candidate biomolecules and/or fragments were identified as either up- or downregulated with a fold change greater than 2 and a p-value below 0.01 in biofilms that were grown on the coated substrates compared to those on uncoated substrates. Metabolomics was performed on biofilms which differed in growth from coated to uncoated substrates. Had normalization by biofilm growth occurred before LC/Q-ToF analysis, the number of metabolites identified as surpassing a twofold change would have likely increased. The complete list of candidates identified here (Table S1) includes phospholipids, quinolones, fatty acids, cardiolipins, and intermediate metabolites in the synthetic pathways of these molecules.

Validation of the Iron-Mediated Design Strategy toward Directed PAO1 Behaviors. To test the design principle and demonstrate that the aforementioned effects were indeed mediated by iron, an array of culture media with varying levels of iron availability were used to grow PAO1 and the resulting levels of pyoverdine/pyocyanin/biofilm growth were analyzed. To achieve iron-excess conditions in which scavenging for iron by PAO1 would be unnecessary, we added  $20~\mu M$  iron(III) chloride to the culture medium prior to inoculation with PAO1. To observe the effect of iron

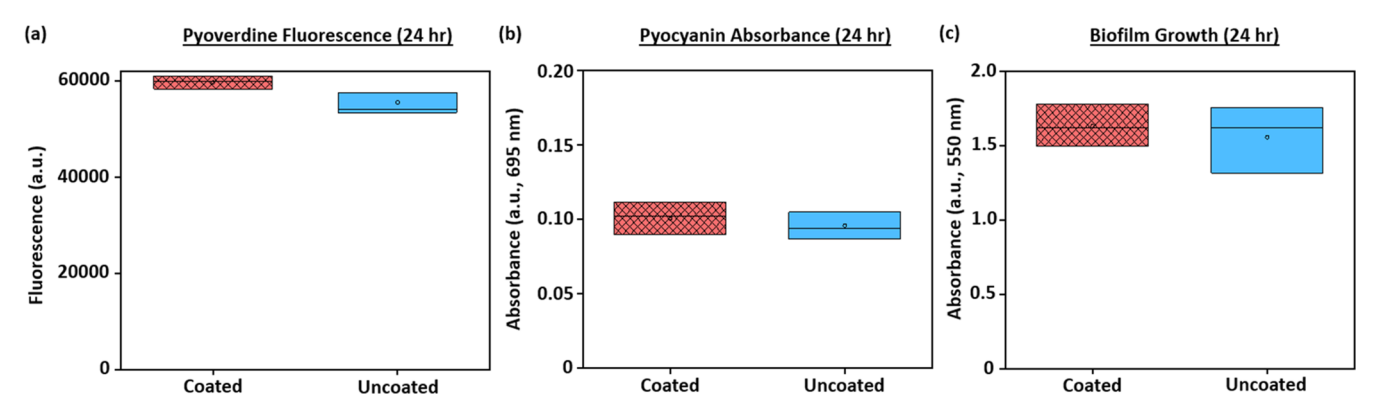


**Figure 6.** Spectroscopic assays quantifying PAO1 pyoverdine and pyocyanin production in iron-depleted medium. (a) Fluorescence of pyoverdine released into culture medium by PAO1 within coated and uncoated microplates in iron-depleted broth (n = 4). (b) Absorbance of pyocyanin released into culture medium by PAO1 within coated and uncoated microplates in iron-depleted broth (n = 4). (c) PAO1 biofilm growth on coated and uncoated substrates in iron-depleted broth (n = 16). Data in (a-c) are represented by an interquartile range (box), median (line), and mean (dot).

deprivation, iron-depleted broth was prepared by the addition of 400  $\mu$ M iron-chelating 2,2′-bipyridyl. These concentrations were chosen to be one to several orders of magnitude greater than the naturally occurring iron concentrations (e.g., over 15  $\mu$ M in human serum).

With excess dissolved iron, the release of pyoverdine (collectively by planktonic cells and biofilms) was diminished to undetectable levels by fluorescence spectroscopy in both coated and uncoated culture conditions (Figure 5a). Pyocyanin release was reduced to 36.22 and 44.01% of the levels measured in the standard medium for coated and uncoated surfaces, respectively, with  $OD_{695}$  values of 0.043  $\pm$  0.015 and  $0.066 \pm 0.0068$  a.u. (Figure 5b). The lower release of pyocyanin by cultures on coated substrates was still observed under iron-excess conditions, likely a result of the multifunctional nature of pyocyanin, which is subject to multiplexed signaling pathways, unlike pyoverdine's predominant association to intracellular iron levels.<sup>61</sup> Biofilm growth under ironexcess conditions closely matched that in the standard medium, with nearly twice as much biofilm formed on the coated surface, confirming the ability of the functional surface to recruit iron and support biofilm growth, the mechanism of which is likely complex and will be an important subject of future studies (Figure 5c). Furthermore, on both surfaces, the biofilms cultured in iron-excess media displayed a distinct increase in organization of a striated pattern, where dense columns containing lines perpendicular to the liquid-air interface (indicated by the double-sided arrows in Figure 5d) were reliably observed. This was likely a result of the known tendency to leave space between 3D clusters creating water channels for the flow of nutrients throughout the biofilm.<sup>62</sup>

In the case of iron deprivation, pyoverdine release was enhanced by 488.76 and 292.41% on coated and uncoated substrates, respectively, compared to those measured in standard medium to values of  $59,615.50 \pm 1661.89$  a.u. and  $55,460.00 \pm 3440.16$  a.u. No statistically significant difference was captured between the two surfaces under iron-deprived conditions (Figure 6a). Similarly, the two surfaces led to similar levels of pyocyanin under iron-deprived conditions, with  $OD_{695}$  values of  $0.10 \pm 0.013$  and  $0.096 \pm 0.012$  a.u., respectively, for the coated and uncoated microplates. These levels signified a slight decrease in pyocyanin release compared to the levels measured in standard medium, which could be a result of the quorum-sensing regulating the production of

pyocyanin, the pathways for which have complex relationships with iron availability and are still being discovered and may be responsible for the decrease in pyocyanin in the iron-deprived environment. We also observed an increase in the growth of biofilms on uncoated substrates to match the quantity on coated substrates when cultured in iron-depleted broth, reaching  $\mathrm{OD}_{550}$  values of  $1.63 \pm 0.44$  and  $1.55 \pm 0.29$  on coated and uncoated surfaces, respectively. One of the numerous driving forces to build a biofilm/sessile state is to more efficiently uptake and ration valuable nutrients (such as iron), which likely drove the high levels of biofilms produced on the uncoated substrates in the case of iron-depleted broth.

The effect of equalized pyoverdine production on coated and uncoated microplates, that is, diminished in iron-excess conditions and enhanced in iron deprivation, validated the iron-mediated design strategy toward directed PAO1 behavior. This iron-regulating functional coating, P4VP-co-DVB, has the potential to become an effective and universal manipulator of PAO1 behavior given the similar iron concentrations in LB medium, groundwater, and many other natural environments. 65,66

# CONCLUSIONS

Biofilms are ubiquitous in nature, and these surface-attached microbial communities are the culprits of issues from disease to fouling of manufacturing equipment. 67,68 Despite their potential for harm, biofilms may also be leveraged for their advantageous qualities of environmental remediation, biotechnological production of consumer goods, or self-powering and self-renewal for living materials. 11,12,69 The fact that biofilms predominantly exist as matrix-enclosed communities attached to a surface dictates an inherent coupling of activity between the bacteria and the solid materials they colonize. Beginning early in the attachment stages, bacteria begin sensing the environment for attachment and qualities such as stiffness, which can dictate the motility of the biofilm-forming bacteria in ways that influence the phenotype and biophysical/ biochemical activities of the biofilm that develops.7 close connection between biofilms and the materials on which they reside demands attention to ways in which the materials can influence the behavior of the biofilms. While most recent studies focused on physical surface features and their connection to bacterial behavior, the relationships between the vast assortment of material chemical properties and

bacteria remain largely unexplored, presenting new opportunities to modulate biofilm phenotypes without the need for genetic modifications.

In this study, we demonstrated how iCVD polymer thin films composed of lightly cross-linked P4VP-co-DVB can change the behavior of biofilm-forming PAO1. This pyridinerich surface material was designed to regulate surface iron availability and was shown to control the behavior of the microbe in predictable ways compared to standard bacteria culture microplates (made of PVC). By coordinating with dissolved iron species, the functional surface reduced the expression and release of siderophores, phenazines, and rhamnolipids, which led to reduced virulence while simultaneously supporting the enhanced growth of biofilms. Other iron-coordinating functionalities will likely have similar effects on the growth and metabolism of biofilms and will be the focus of our future research. While the impact of soluble species has been studied extensively for PAO1 biofilms, the impact of materials surface chemistries remains largely elusive beyond antifouling or antimicrobial effects. 72,73 These results serve as proof-of-principle for the capability of materials-chemistrybased modulation of biofilms, pointing to a transformative design strategy for functional and living materials where the microbial behavior/phenotype is manipulated via molecularly engineered environments. Future work will systematically unravel the relationships between microbial behavior/phenotype and material properties, charting the landscape of material-centric biomolecular engineering. This strategy is promising, especially given the emerging understanding that biofilm formation is not only a common trait but also the dominant mode of bacterial growth in nature. To build upon these results, future functional materials may be designed to attract, but not sequester, key soluble molecules to influence the metabolism, communal signaling, or even symbiosis with eukaryotic systems of a broad range of microbes, pointing to a future where living materials can be integrated into everyday

## ASSOCIATED CONTENT

# **5** Supporting Information

The Supporting Information is available free of charge at https://pubs.acs.org/doi/10.1021/acs.biomac.1c00731.

NMR analysis of P4VP-co-DVB coating stability, schematic of a custom iCVD reactor, SEM imaging of the P4VP-co-DVB thin film on the microplate substrate, FTIR analysis and composition determination of the P4VP-co-DVB thin film, FTIR spectrum and deposition conditions of PDVB thin film, PAO1 culture color on coated and uncoated substrates, quantification of iron enriched to surfaces of coated and uncoated microplates, spectroscopic assays quantifying PAO1 pyoverdine and pyocyanin production and biofilm growth on PDVB, mass spectrometry analysis confirming selected molecules, and raw metabolomics data comparing biofilms grown on coated versus uncoated substrates (PDF)

# AUTHOR INFORMATION

## **Corresponding Authors**

Sijin Li – Robert F. Smith School of Chemical & Biomolecular Engineering, Cornell University, Ithaca, New York 14853, United States; orcid.org/0000-0003-0364-5632; Email: sijin.li@cornell.edu

Rong Yang — Robert F. Smith School of Chemical & Biomolecular Engineering, Cornell University, Ithaca, New York 14853, United States; orcid.org/0000-0001-6427-026X; Email: ryang@cornell.edu

#### **Authors**

Trevor Franklin — Robert F. Smith School of Chemical & Biomolecular Engineering, Cornell University, Ithaca, New York 14853, United States

Yinan Wu — Robert F. Smith School of Chemical & Biomolecular Engineering, Cornell University, Ithaca, New York 14853, United States

Jiayan Lang — Robert F. Smith School of Chemical & Biomolecular Engineering, Cornell University, Ithaca, New York 14853, United States; orcid.org/0000-0002-0865-2690

Complete contact information is available at: https://pubs.acs.org/10.1021/acs.biomac.1c00731

#### **Author Contributions**

The manuscript was written through the contributions of all authors. All authors have given approval to the final version of the manuscript.

#### Notes

The authors declare no competing financial interest.

#### ACKNOWLEDGMENTS

The authors acknowledge the National Institutes of Health -National Institute on Deafness and Other Communication Disorders for support (NIHDC016644 to R.Y.). Furthermore, the project was sponsored by the Department of the Navy, Office of Naval Research under ONR award N00014-20-1-2418. This material is based upon work supported by the National Science Foundation Graduate Research Fellowship Program under grant no. DGE-1650441. Any opinions, findings, conclusions, or recommendations expressed in this material are those of the author(s) and do not necessarily reflect the views of the National Science Foundation. Analytical methods involved the use of the Cornell Center for Materials Research (CCMR) Shared Facilities, which are supported through the NSF MRSEC program (DMR-1719875). We thank the Trace Elements Clean Lab at the University of Wisconsin-Madison Wisconsin State Laboratory of Hygiene for support with ICP-MS measurements. We thank A. Hay for discussions on experimental design and data analysis, as well as J. Grazul for support with biofilm SEM preparation, G. Swan for assistance in the design of temperature control materials, and A. Condo for support with NMR.

### REFERENCES

- (1) Siboni, N.; Lidor, M.; Kramarsky-Winter, E.; Kushmaro, A. Conditioning Film and Initial Biofilm Formation on Ceramics Tiles in the Marine Environment. *FEMS Microbiol. Lett.* **2007**, *274*, 24–29.
- (2) Flemming, H.-C.; Wingender, J.; Szewzyk, U.; Steinberg, P.; Rice, S. A.; Kjelleberg, S. Biofilms: an emergent form of bacterial life. *Nat. Rev. Microbiol.* **2016**, *14*, 563–575.
- (3) Ross, A. M.; Lahann, J. Current Trends and Challenges in Biointerfaces Science and Engineering. *Annu. Rev. Chem. Biomol. Eng.* **2015**, *6*, 161–186.
- (4) Ratner, B. D. Biomaterials: Been There, Done That, and Evolving into the Future. *Annu. Rev. Biomed. Eng.* **2019**, 21, 171–191.

- (5) Ma, Y.; Tian, X.; Liu, L.; Pan, J.; Pan, G. Dynamic Synthetic Biointerfaces: From Reversible Chemical Interactions to Tunable Biological Effects. *Acc. Chem. Res.* **2019**, *52*, 1611–1622.
- (6) Chang, H.-I. Cell Responses to Surface and Architecture of Tissue Engineering Scaffolds. In Regenerative Medicine and Tissue Engineering—Cells and Biomaterials; Eberli, D., Ed.; IntechOpen: Rijeka, 2011.
- (7) Flemming, H.-C.; Wuertz, S. Bacteria and Archaea on Earth and Their Abundance in Biofilms. *Nat. Rev. Microbiol.* **2019**, *17*, 247–260.
- (8) Yang, R.; Jang, H.; Stocker, R.; Gleason, K. K. Synergistic Prevention of Biofouling in Seawater Desalination by Zwitterionic Surfaces and Low-Level Chlorination. *Adv. Mater.* **2014**, *26*, 1711–1718
- (9) Whitesides, G. M. Soft Robotics. Angew. Chem. Int. Ed. 2018, 57, 4258-4273.
- (10) Steltz, E.; Mozeika, A.; Rembisz, J.; Corson, N.; Jaeger, H. M. Jamming as an Enabling Technology for Soft Robotics. *Proceedings SPIE 7642, Electroactive Polymer Actuators and Devices (EAPD)*, San Diego, CA, 2010; Vol. 7642.
- (11) Berlanga, M.; Guerrero, R. Living Together in Biofilms: The Microbial Cell Factory and Its Biotechnological Implications. *Microb. Cell Factories* **2016**, *15*, 165.
- (12) Jagmann, N.; Philipp, B. Design of Synthetic Microbial Communities for Biotechnological Production Processes. *J. Biotechnol.* **2014**, *184*, 209–218.
- (13) McKay, R.; Ghodasra, M.; Schardt, J.; Quan, D.; Pottash, A. E.; Shang, W.; Jay, S. M.; Payne, G. F.; Chang, M. W.; March, J. C.; Bentley, W. E. A Platform of Genetically Engineered Bacteria as Vehicles for Localized Delivery of Therapeutics: Toward Applications for Crohn's Disease. *Bioeng. Transl. Med.* **2018**, *3*, 209–221.
- (14) Singh, J. S.; Abhilash, P. C.; Singh, H. B.; Singh, R. P.; Singh, D. P. Genetically Engineered Bacteria: An Emerging Tool for Environmental Remediation and Future Research Perspectives. *Gene* **2011**, 480, 1–9.
- (15) Prakash, D.; Verma, S.; Bhatia, R.; Tiwary, B. N. Risks and Precautions of Genetically Modified Organisms. *ISRN Ecol.* **2011**, 2011, 369573.
- (16) Shchukin, D. G.; Möhwald, H. Self-Repairing Coatings Containing Active Nanoreservoirs. *Small* **2007**, *3*, 926–943.
- (17) Heveran, C. M.; Williams, S. L.; Qiu, J.; Artier, J.; Hubler, M. H.; Cook, S. M.; Cameron, J. C.; Srubar, W. V. Biomineralization and Successive Regeneration of Engineered Living Building Materials. *Matter* **2020**, *2*, 481–494.
- (18) Levin, P. A.; Angert, E. R. Small but Mighty: Cell Size and Bacteria. Cold Spring Harbor Perspect. Biol. 2015, 7, a019216.
- (19) Li, S.; Li, Y.; Smolke, C. D. Strategies for Microbial Synthesis of High-Value Phytochemicals. *Nat. Chem.* **2018**, *10*, 395–404.
- (20) Magana, M.; Sereti, C.; Ioannidis, A.; Mitchell, C. A.; Ball, A. R.; Magiorkinis, E.; Chatzipanagiotou, S.; Hamblin, M. R.; Hadjifrangiskou, M.; Tegos, G. P. Options and Limitations in Clinical Investigation of Bacterial Biofilms. *Clin. Microbiol. Rev.* **2018**, *31*, e00084–16.
- (21) Sarjit, A.; Tan, S. M.; Dykes, G. A. Surface Modification of Materials to Encourage Beneficial Biofilm Formation. *AIMS Bioeng.* **2015**, *2*, 404–422.
- (22) Song, F.; Ren, D. Stiffness of Cross-Linked Poly-(Dimethylsiloxane) Affects Bacterial Adhesion and Antibiotic Susceptibility of Attached Cells. *Langmuir* **2014**, *30*, 10354–10362.
- (23) Makarchuk, S.; Braz, V. C.; Araújo, N. A. M.; Ciric, L.; Volpe, G. Enhanced Propagation of Motile Bacteria on Surfaces Due to Forward Scattering. *Nat. Commun.* **2019**, *10*, 4110.
- (24) Ratledge, Č.; Dover, L. G. Iron Metabolism in Pathogenic Bacteria. *Annu. Rev. Microbiol.* **2000**, *54*, 881–941.
- (25) Kramer, J.; Özkaya, Ö.; Kümmerli, R. Bacterial Siderophores in Community and Host Interactions. *Nat. Rev. Microbiol.* **2020**, *18*, 152–163
- (26) Rue, E.; Bruland, K. Domoic Acid Binds Iron and Copper: A Possible Role for the Toxin Produced by the Marine Diatom Pseudo-Nitzschia. *Mar. Chem.* **2001**, *76*, 127–134.

- (27) Wilson, B. R.; Bogdan, A. R.; Miyazawa, M.; Hashimoto, K.; Tsuji, Y. Siderophores in Iron Metabolism: From Mechanism to Therapy Potential. *Trends Mol. Med.* **2016**, 22, 1077–1090.
- (28) Kang, D.; Kirienko, N. V. High-Throughput Genetic Screen Reveals That Early Attachment and Biofilm Formation Are Necessary for Full Pyoverdine Production by Pseudomonas Aeruginosa. *Front. Microbiol.* **2017**, *8*, 1707.
- (29) Donadt, T. B.; Yang, R. Vapor-Deposited Biointerfaces and Bacteria: An Evolving Conversation. *ACS Biomater. Sci. Eng.* **2020**, *6*, 182–197.
- (30) Coclite, A. M.; Howden, R. M.; Borrelli, D. C.; Petruczok, C. D.; Yang, R.; Yagüe, J. L.; Ugur, A.; Chen, N.; Lee, S.; Jo, W. J.; Liu, A.; Wang, X.; Gleason, K. K. 25th Anniversary Article: CVD Polymers: A New Paradigm for Surface Modifi Cation and Device Fabrication. *Adv. Mater.* 2013, 25, 5392–5423.
- (31) Alf, M. E.; Asatekin, A.; Barr, M. C.; Baxamusa, S. H.; Chelawat, H.; Ozaydin-Ince, G.; Petruczok, C. D.; Sreenivasan, R.; Tenhaeff, W. E.; Trujillo, N. J.; Vaddiraju, S.; Xu, J.; Gleason, K. K. Chemical Vapor Deposition of Conformal, Functional, and Responsive Polymer Films. *Adv. Mater.* **2010**, *22*, 1993–2027.
- (32) Wu, D. C.; Chan, W. W.; Metelitsa, A. I.; Fiorillo, L.; Lin, A. N. Pseudomonas Skin Infection. *Am. J. Clin. Dermatol.* **2011**, *12*, 157–169
- (33) Young, M.; Ozcan, A.; Lee, B.; Maxwell, T.; Andl, T.; Rajasekaran, P.; Beazley, M. J.; Tetard, L.; Santra, S. N-Acetyl Cysteine Coated Gallium Particles Demonstrate High Potency against Pseudomonas Aeruginosa PAO1. *Pathogens* **2019**, *8*, 120.
- (34) Tautenhahn, R.; Patti, G. J.; Rinehart, D.; Siuzdak, G. XCMS Online: A Web-Based Platform to Process Untargeted Metabolomic Data. *Anal. Chem.* **2012**, *84*, 5035–5039.
- (35) Cornelis, P.; Dingemans, J. Pseudomonas Aeruginosa Adapts Its Iron Uptake Strategies in Function of the Type of Infections. *Front. Cell. Infect. Microbiol.* **2013**, *3*, 75.
- (36) Gleason, K. K. Overview of Chemically Vapor Deposited (CVD) Polymers. In *CVD Polymers*; Gleason, K. K., Ed.; Wiley Online Books, 2015.
- (37) Petruczok, C. D.; Yang, R.; Gleason, K. K. Controllable Cross-Linking of Vapor-Deposited Polymer Thin Films and Impact on Material Properties. *Macromolecules* **2013**, *46*, 1832–1840.
- (38) Rasamiravaka, T.; Labtani, Q.; Duez, P.; El Jaziri, M. The Formation of Biofilms by Pseudomonas Aeruginosa: A Review of the Natural and Synthetic Compounds Interfering with Control Mechanisms. *BioMed Res. Int.* **2015**, 2015, 759348.
- (39) Donadt, T. B.; Yang, R. Amphiphilic Polymer Thin Films with Enhanced Resistance to Biofilm Formation at the Solid—Liquid—Air Interface. *Adv. Mater. Interfaces* **2021**, *8*, 2001791.
- (40) O'Toole, G. A. Microtiter Dish Biofilm Formation Assay. *J. Visualized Exp.* **2011**, *47*, No. e2437.
- (41) Banin, E.; Vasil, M. L.; Greenberg, E. P. Iron and Pseudomonas Aeruginosa Biofilm Formation. *Proc. Natl. Acad. Sci. U.S.A.* **2005**, *102*, 11076–11081.
- (42) Sha, J.; Pillai, L.; Fadl, A. A.; Galindo, C. L.; Erova, T. E.; Chopra, A. K. The Type III Secretion System and Cytotoxic Enterotoxin Alter the Virulence of Aeromonas Hydrophila. *Infect. Immun.* **2005**, *73*, 6446–6457.
- (43) Christiaen, S. E. A.; Matthijs, N.; Zhang, X.-H.; Nelis, H. J.; Bossier, P.; Coenye, T. Bacteria That Inhibit Quorum Sensing Decrease Biofilm Formation and Virulence in Pseudomonas Aeruginosa PAO1. *Pathog. Dis.* **2014**, *70*, 271–279.
- (44) Kirienko, D. R.; Kang, D.; Kirienko, N. V. Novel Pyoverdine Inhibitors Mitigate Pseudomonas Aeruginosa Pathogenesis. *Front. Microbiol.* **2019**, *9*, 3317.
- (45) Bonneau, A.; Roche, B.; Schalk, I. J. Iron Acquisition in Pseudomonas Aeruginosa by the Siderophore Pyoverdine: An Intricate Interacting Network Including Periplasmic and Membrane Proteins. *Sci. Rep.* **2020**, *10*, 120.
- (46) Page, M. G. P. The Role of Iron and Siderophores in Infection, and the Development of Siderophore Antibiotics. *Clin. Infect. Dis.* **2019**, *69*, S529—S537.

- (47) Cox, C. D. Role of Pyocyanin in the Acquisition of Iron from Transferrin. *Infect. Immun.* **1986**, *52*, 263–270.
- (48) Jayaseelan, S.; Ramaswamy, D.; Dharmaraj, S. Pyocyanin: Production, Applications, Challenges and New Insights. *World J. Microbiol. Biotechnol.* **2014**, *30*, 1159–1168.
- (49) Lau, G. W.; Hassett, D. J.; Ran, H.; Kong, F. The Role of Pyocyanin in Pseudomonas Aeruginosa Infection. *Trends Mol. Med.* **2004**, *10*, 599–606.
- (50) Nose, H.; Rodgers, M. T. Influence of the d Orbital Occupation on the Structures and Sequential Binding Energies of Pyridine to the Late First-Row Divalent Transition Metal Cations: A DFT Study. *J. Phys. Chem. A* **2014**, *118*, 8129–8140.
- (51) Bhagwat, G.; O'Connor, W.; Grainge, I.; Palanisami, T. Understanding the Fundamental Basis for Biofilm Formation on Plastic Surfaces: Role of Conditioning Films. *Front. Microbiol.* **2021**, *12*, 687118.
- (52) Ren, Y.; Wang, C.; Chen, Z.; Allan, E.; van der Mei, H. C.; Busscher, H. J. Emergent Heterogeneous Microenvironments in Biofilms: Substratum Surface Heterogeneity and Bacterial Adhesion Force-Sensing. FEMS Microbiol. Rev. 2018, 42, 259–272.
- (53) Rummel, C. D.; Lechtenfeld, O. J.; Kallies, R.; Benke, A.; Herzsprung, P.; Rynek, R.; Wagner, S.; Potthoff, A.; Jahnke, A.; Schmitt-Jansen, M. Conditioning Film and Early Biofilm Succession on Plastic Surfaces. *Environ. Sci. Technol.* **2021**, *55*, 11006–11018.
- (54) Cézard, C.; Sonnet, P.; Bouvier, B. Ironing out Pyoverdine's Chromophore Structure: Serendipity or Design? *J. Biol. Inorg. Chem.* **2019**, 24, 659–673.
- (55) Kang, D.; Kirienko, N. V. Interdependence between Iron Acquisition and Biofilm Formation in Pseudomonas Aeruginosa. *J. Microbiol.* **2018**, *56*, 449–457.
- (56) Wang, Y.; Wilks, J. C.; Danhorn, T.; Ramos, I.; Croal, L.; Newman, D. K. Phenazine-1-Carboxylic Acid Promotes Bacterial Biofilm Development via Ferrous Iron Acquisition. *J. Bacteriol.* **2011**, 193, 3606–3617.
- (57) Köhler, T.; Guanella, R.; Carlet, J.; van Delden, C. Quorum Sensing-Dependent Virulence during Pseudomonas Aeruginosa Colonisation and Pneumonia in Mechanically Ventilated Patients. *Thorax* **2010**, *65*, 703–710.
- (58) Glick, R.; Gilmour, C.; Tremblay, J.; Satanower, S.; Avidan, O.; Déziel, E.; Greenberg, E. P.; Poole, K.; Banin, E. Increase in Rhamnolipid Synthesis under Iron-Limiting Conditions Influences Surface Motility and Biofilm Formation in Pseudomonas Aeruginosa. *J. Bacteriol.* **2010**, *192*, 2973–2980.
- (59) Boles, B. R.; Thoendel, M.; Singh, P. K. Rhamnolipids Mediate Detachment of PseudomonasAeruginosa from Biofilms. *Mol. Microbiol.* **2005**, *57*, 1210–1223.
- (60) Shen, X.; Yang, H.; Zhang, D.; Jiang, H. Iron Concentration Does Not Differ in Blood but Tends to Decrease in Cerebrospinal Fluid in Parkinson's Disease. *Front. Neurosci.* **2019**, *13*, 939.
- (61) Visaggio, D.; Pasqua, M.; Bonchi, C.; Kaever, V.; Visca, P.; Imperi, F. Cell Aggregation Promotes Pyoverdine-Dependent Iron Uptake and Virulence in Pseudomonas Aeruginosa. *Front. Microbiol.* **2015**, *6*, 902.
- (62) Davey, M. E.; Caiazza, N. C.; O'Toole, G. A. Rhamnolipid Surfactant Production Affects Biofilm Architecture in Pseudomonas Aeruginosa PAO1. *J. Bacteriol.* **2003**, *185*, 1027–1036.
- (63) O'Loughlin, C. T.; Miller, L. C.; Siryaporn, A.; Drescher, K.; Semmelhack, M. F.; Bassler, B. L. A Quorum-Sensing Inhibitor Blocks Pseudomonas Aeruginosa Virulence and Biofilm Formation. *Proc. Natl. Acad. Sci. U.S.A.* **2013**, *110*, 17981–17986.
- (64) Sun, F.; Li, N.; Wang, L.; Feng, H.; Shen, D.; Wang, M. Iron Interferes with Quorum Sensing-Mediated Cooperation in Pseudomonas Aeruginosa by Affecting the Expression of PpyR and MexT, in Addition to RhlR. *J. Microbiol.* **2020**, *58*, 938–944.
- (65) Sharma, S. K.; Petrusevski, B.; Schippers, J. C. Biological Iron Removal from Groundwater: A Review. *J. Water Supply Res. Technol.* **2005**, *54*, 239–247.

- (66) Avery, A. M.; Goddard, H. J.; Sumner, E. R.; Avery, S. V. Iron Blocks the Accumulation and Activity of Tetracyclines in Bacteria. *Antimicrob. Agents Chemother.* **2004**, *48*, 1892–1894.
- (67) Del Pozo, J. L. Biofilm-related disease. Expert Rev. Anti Infect. Ther. 2018, 16, 51–65.
- (68) Galié, S.; García-Gutiérrez, C.; Miguélez, E. M.; Villar, C. J.; Lombó, F. Biofilms in the Food Industry: Health Aspects and Control Methods. *Front. Microbiol.* **2018**, *9*, 898.
- (69) Nguyen, P. Q.; Courchesne, N.-M. D.; Duraj-Thatte, A.; Praveschotinunt, P.; Joshi, N. S. Engineered Living Materials: Prospects and Challenges for Using Biological Systems to Direct the Assembly of Smart Materials. *Adv. Mater.* **2018**, *30*, 1704847.
- (70) Craig, L.; Forest, K. T.; Maier, B. Type IV Pili: Dynamics, Biophysics and Functional Consequences. *Nat. Rev. Microbiol.* **2019**, 17, 429–440.
- (71) Song, F.; Koo, H.; Ren, D. Effects of Material Properties on Bacterial Adhesion and Biofilm Formation. *J. Dent. Res.* **2015**, *94*, 1027–1034.
- (72) Wibowo, J. P.; Batista, F. A.; van Oosterwijk, N.; Groves, M. R.; Dekker, F. J.; Quax, W. J. A Novel Mechanism of Inhibition by Phenylthiourea on PvdP, a Tyrosinase Synthesizing Pyoverdine of Pseudomonas Aeruginosa. *Int. J. Biol. Macromol.* **2020**, *146*, 212–221. (73) Kronda, I. M.; Cooper, R. A.; Maddocks, S. E. Manuka Honey
- (73) Kronda, J. M.; Cooper, R. A.; Maddocks, S. E. Manuka Honey Inhibits Siderophore Production in Pseudomonas Aeruginosa. *J. Appl. Microbiol.* **2013**, *115*, 86–90.